Enhancing System Performance in Subsea and Off-Highway Applications: A High-Fidelity, Transient Dynamic CFD Analysis Approach

Vignesh Jeganathan[1,*], Rayhan Ahmed[1], Yawei Chen[1], Shyam Sundar Pasunurthi[1], Ashutosh Pandey[1], Emanuele Gnesi[2], Raju Kalidindi[2], Bipin Kashid[2], Howard Zhang[2]

[1]*Simerics, Inc.*
[2]*Parker Hannifin Corporation*
[*]*Corresponding Author, E-mail:* `vj@simerics.com`

Abstract

In hydraulic fluid power engineering, the need for reliability and high efficiency in system components, including valves and pumps, is paramount. This requirement becomes even more critical in tough operational environments, such as off-highway and subsea applications, which require both robust durability and optimal operational efficiency. Computational Fluid Dynamics (CFD) simulations are often used to address these demands and assume a pivotal role during product development. This paper demonstrates the use of CFD simulations as a tool to study the operations of a solenoid valve and a vane pump, which are used in subsea and off-highway applications. Our research employs 3D CFD simulations to examine complex transient dynamic phenomena such as two-piece poppet separation in solenoid valves and vane translation in the vane slots of vane pumps. By modeling these complex transient dynamics, we illustrate how CFD can identify problems that are difficult to test experimentally, and offer valuable insights for enhancing performance.

Keywords: subsea, off-highway, valves, vane pumps, CFD, cavitation, performance prediction, design improvement.

River Journal, 1–27.

1 Introduction

Hydraulic systems are the critical infrastructure behind a wide array of industrial operations, powering machinery across the demanding landscapes of off-highway and subsea applications. The cornerstone of the effectiveness of these systems lies in the performance, reliability, and efficiency of key components, particularly pumps and valves. The pump is the main driving component that delivers the high pressure working fluid for the desired function of an hydraulic system, whereas the valves act as working fluid control components. The complexity of fluid behaviors and transient dynamics present in these components presents a significant challenge, often outpacing the capabilities of traditional design and testing methodologies to predict and mitigate issues that could undermine component functionality.

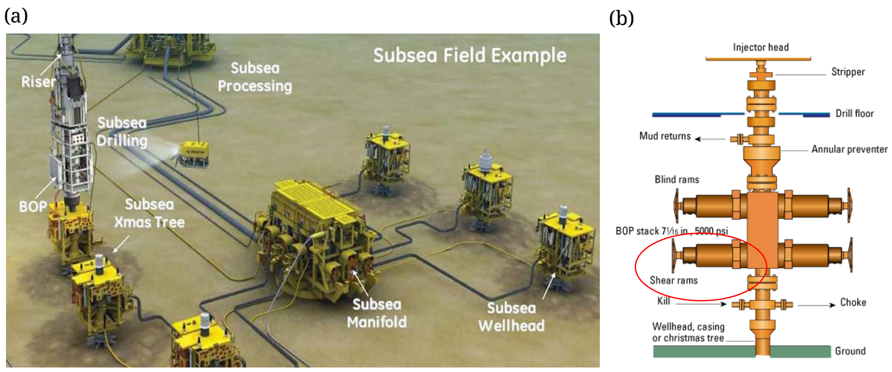

Figure 1 Components of (a) a subsea production system showing a Blow-Out Preventer (BOP), and (b) a BOP. Red circle highlights the shear ram which contains a pilot valve as one of its components.

The primary design criteria for components are determined by their unique applications and the variations among them. The components used in subsea applications (figure. 1 a) are required to resist extreme corrosive sea conditions, high deep-sea pressures, and severe temperatures, while also maintaining high levels of reliability and efficiency [1]. A range of proven and validated best practices [2–4] guide the design process of subsea valves and pump components. Off-highway hydraulic systems (figure. 2 a), which are used in sectors such as agriculture, construction, earth moving and material handling, have their unique design requirements. Given the substantial role of off-highway applications in total greenhouse gas emissions, it is crucial to minimize fuel costs and emissions. Therefore, there are ongoing efforts to create cost-effective electric-hydraulic systems [5–7].

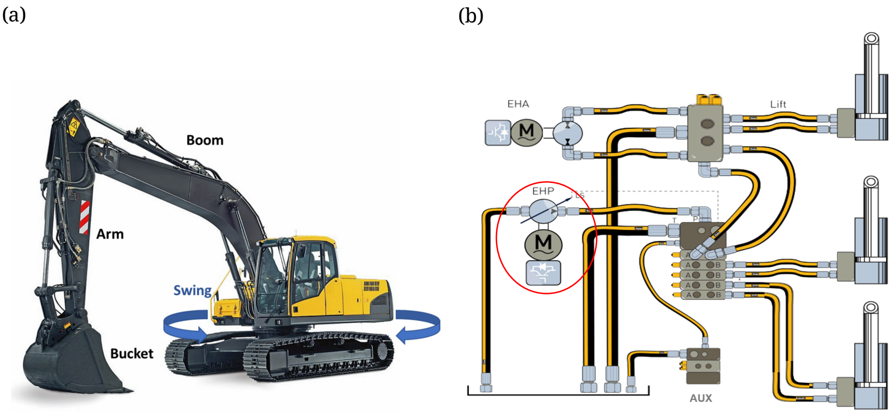

Figure 2 Schematic of (a) an off-highway equipment [7] and (b) hydraulic system used in the off-highway equipment. Red circle highlights the positive displacement pump studied in the current work.

In addition to adhering to design standards, it is crucial to optimize a component's fluid flow characteristics to ensure the optimal operation of both subsea and offshore equipment, considering their rigorous demands. CFD has been instrumental in achieving this for many years. A detailed investigation [8] using CFD on ball check valves has underscored the impact of cavitation on flow under varying pressure drop scenarios across the valve. Notably, it has revealed that the flow coefficient is not fixed but depends on the cavitation number. In a computational study of subsea safety valves [9], the integration of CFD with nonlinear finite element analysis (FEA) simulations has provided insight into the stresses triggered by high-pressure solid substances that could exceed design thresholds. The functionality of a two-way control valve in a hydraulic system is enhanced by applying CFD [10]. CFD has also been used to investigate the functioning of a double-acting vane pump, which incorporates vane dynamics [11], which has applicable benefits in power split transmission systems.

Parker Hannifin adopts an all-encompassing multiphysics simulation strategy to meticulously scrutinize and optimize hydraulic systems. Our methodology integrates 1D, FEA, 3D FEA, and CFD simulations, supplemented by co-simulations and proactive simulation-guided optimization studies. Central to our approach is a rigorous validation and verification framework, which ensures that our simulations serve as accurate proxies for real-world performance [12]. This paper aims to showcase our endeavor to explore the intricate transient dynamic behavior of a solenoid valve and a vane pump, driven by flow, using the sophisticated 3D CFD software, Simerics MP+.

The solenoid valve presented in this study is a part of the shear ram, which in turn is an integral part of a Blow-Out Preventer (BOP) [13]. A BOP (as shown in the figure. 1 b) is a device used in subsea systems to prevent crude oil or natural gas from spilling uncontrollably from a well. In this paper, we study this specific solenoid valve also called the pilot valve for cavitation and valve body forces. The primary challenge addressed is the phenomenon of two-piece valve body separation during valve travel, a complex transient dynamic behavior difficult to predict and optimize in experiments.

The second device, a vane pump, is used in an off-highway electric-hydraulic mobile system, specifically coupled with an electric motor as shown in the figure. 2 b. In this section, our aim is to discuss the cavitation and flow characteristics of a vane pump design. after meticulous modeling of transient dynamics, such as vane motion within the slots.

1.1 Solenoid valve

The solenoid valve we discuss in the paper is solenoid operated and is shown in figure. 3a. The valve body comprises three disconnected parts: a solenoid, a pin, and a poppet whose diameters are around 0.2 m. The poppet is the actual body that seals the ports. The solenoid and poppet have pre-compressed springs that tend to push them inward towards the center of the valve. When the solenoid is deactivated, the spring forces position the valve bodies onto the right valve seat, meaning the right poppet seat blocks the flow between the inlet and intermediate pressure ports. This also connects the intermediate and outlet ports. When the solenoid is actuated to add additional force, the valve bodies move from right to left, and the left poppet seat sits on the left valve seat, sealing the intermediate port and the outlet, meanwhile, enabling the flow between the inlet and the intermediate ports. The spring and solenoid actuation forces are outlined in the free-body diagram depicted in the figure. 3b. The valve uses 95% water and 5% glycol mixture as a working fluid at 25 °C, whose properties are similar to water. The saturation pressure of this mixture is 3.169 kPa, which is required for cavitation study. The inlet is kept constantly at high pressure of 22.6 MPa, while the outlet is kept at atmospheric pressure of 101 kPa. The intermediate port is spring loaded and

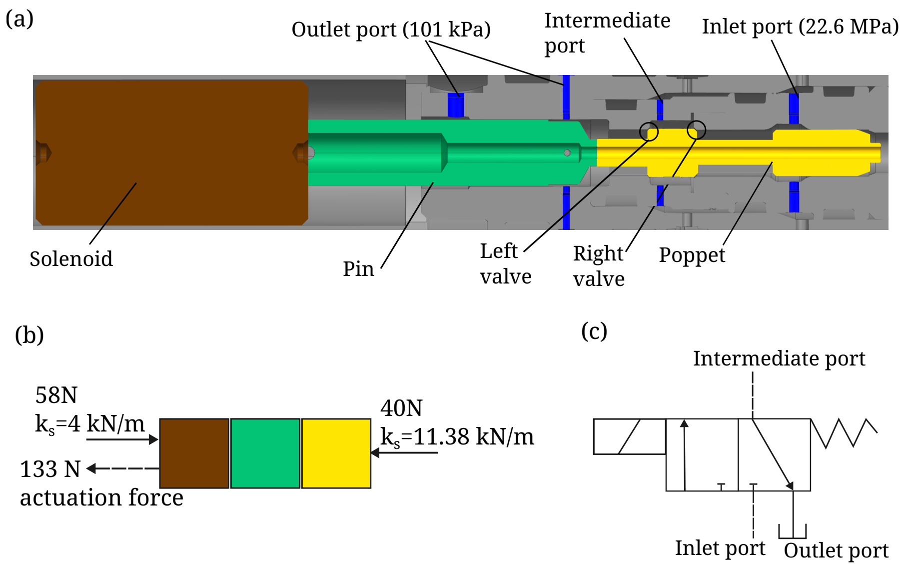

Figure 3 (a) Cross section of solenoid operated valve showing valve bodies and ports. (b) Free-body diagram showing the spring and solenoid forces, and the spring constants. (c) Hydraulic symbol of the pilot valve.

is either at high or atmospheric pressure depending on the position of the poppet. The valve can be represented using a hydraulic symbol as shown in figure. 3c.

1.2 Vane pump

The vane pump shown in figure. 4 comprises of a few parts: the inlet, the outlet, and the rotor chamber that houses the rotor and the vanes. The rotor has a radius of approximately 2.275×10^{-2} m. As the rotor rotates, the fluid is pressurized and displaced from the inlet to the outlet by vanes. The vanes move radially back and forth inside the vane slots based on pressure, spring, and centrifugal forces. The fluid volume inside the rotor chamber that depicts vane fluid volumes and cam profiles is shown in the figure. 4 b. The silicone fluid at 45 °C with a density of 857 kg.m^{-3} and a viscosity of 2.742 $\times10^{-2}$ Pa.s is used as a working fluid. The saturation pressure required for cavitation study is set to be 133 Pa.

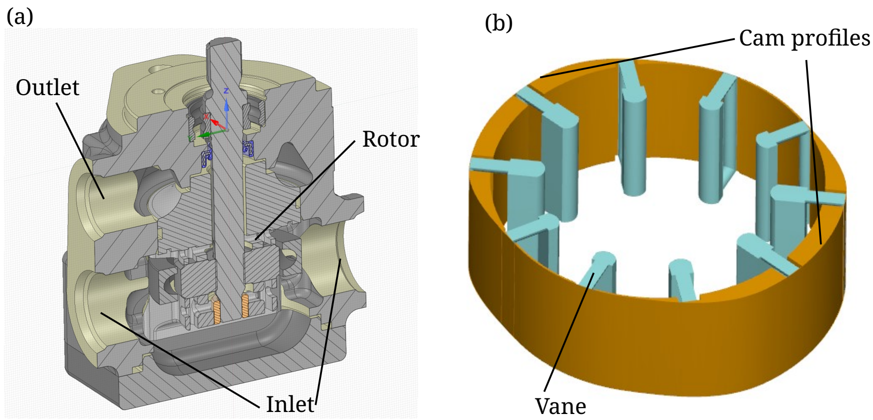

Figure 4 (a) Cross section of vane pump assembly. (b) Fluid volume enclosed in the rotor chamber

2 Numerical models

2.1 Computational Fluid Dynamics model

In a CFD simulation, Navier-Stokes equations that govern the fluid flow are solved numerically to determine the fluid velocity and pressure in the system.

The spatially averaged mass and momentum conservation equations can be written in integral form as follows:

$$\frac{\partial}{\partial t}\int_{\Omega(t)} \rho d\Omega + \int_{\sigma} \rho(v - v_{\sigma}).nd\sigma = 0, \tag{1}$$

and

$$\frac{\partial}{\partial t}\int_{\Omega(t)} \rho v d\Omega + \int_{\sigma} \rho v((v - v_{\sigma}).n)d\sigma = \int_{\sigma} \tau.nd\sigma - \int_{\sigma} Pnd\sigma + \int_{\Omega} fd\Omega. \tag{2}$$

In the above equations, ρ is density of the working fluid, v is spatially averaged velocity vector, v_{σ} is velocity of a moving reference frame, τ is deviatoric stress tensor, P is the pressure and f represents the body force e.g. gravity. σ and Ω under the integral represent the surface and volume integrals respectively.

The standard $\kappa - \epsilon$ two equation model with wall function is used to account for turbulence as follows:

$$\frac{\partial}{\partial t}\int_{\Omega(t)}\rho\kappa d\Omega+\int_{\sigma}\rho((v-v_{\sigma}).n)\kappa d\sigma=\int_{\sigma}(\mu+\frac{\mu_t}{\sigma_{\kappa}})(\bigtriangledown\kappa.n)d\sigma + \int_{\Omega}(G_t-\rho\epsilon)d\Omega, \quad (3)$$

and

$$\frac{\partial}{\partial t}\int_{\Omega(t)}\rho\epsilon d\Omega+\int_{\sigma}\rho((v-v_{\sigma}).n)\epsilon d\sigma = \int_{\sigma}(\mu+\frac{\mu_t}{\sigma_{\epsilon}})(\bigtriangledown\epsilon.n)d\sigma+\int_{\Omega}(c_1G_t\frac{\epsilon}{\kappa}-c_2\rho\frac{\epsilon^2}{\kappa})d\Omega. \quad (4)$$

κ is spatially averaged turbulent kinetic energy, ϵ is spatially averaged dissipation of turbulent kinetic energy, μ_t is turbulent viscosity, c_1 and c_2 are model constants, and G_t is a turbulent kinetic energy production source term.

To account for cavitation/aeration, the cavitation model proposed by Singhal et. al. [14] is implemented in Simerics-MP+. It accounts for real liquid properties, cavitation, aeration, and liquid compressibility. The following formulation describes the cavitation vapor distribution.

$$\frac{\partial}{\partial t}\int_{\Omega(t)}\rho f_v d\Omega+\int_{\sigma}\rho((v-v_{\sigma}).n)f_v d\sigma=\int_{\sigma}(D_{f_v}+\frac{\mu_c}{\sigma_{f_v}})(\bigtriangledown f_v.n)d\sigma + \int_{\Omega}(R_e-R_c)d\Omega \quad (5)$$

Where, f_v is volume fraction of vapor of the working fluid, D_f is the diffusivity of the vapor mass fraction and σ_f is the turbulent Schmidt number. In the present study, these two numbers are set equal to the mixture viscosity and unity, respectively. The vapor generation term, R_e and the condensation rate, R_c are modelled as follows:

$$R_e=C_e\frac{\sqrt{K}}{\sigma_l}\rho_l\rho_v\left(\frac{2}{3}\frac{(p-p_v)}{\rho_l}\right)^{1/2}(1-f_v-f_g) \quad (6)$$

$$R_c=C_c\frac{\sqrt{K}}{\sigma_l}\rho_l\rho_v\left(\frac{2}{3}\frac{(p-p_v)}{\rho_l}\right)^{1/2}(f_v) \quad (7)$$

Where, model constants are $C_e = 0.02$ and $C_c = 0.01$. The final density calculation for the mixture is done by,

$$\frac{1}{\rho} = \frac{f_v}{\rho_v} + \frac{f_g}{\rho_g} + \frac{1 - f_v - f_g}{\rho_l} \tag{8}$$

Non-condensable gas (NCG) is considered as either a free gas or a combination of free gas and dissolved gas. Different models are implemented in Simerics-MP+ that account for both the components of NCG. More details are available in the software manual [15]. In the solenoid valve simulation, the constant gas mass fraction model is used which only captures the free gas component of the air. An equilibrium dissolved gas model is used in the simulation of the vane pump. The model captures both the free and the dissolved components of the air.

The above set of equations is discretized using a finite volume approach and solved using a pressure-based solution algorithm. Spatial terms and temporal terms are handled using second order upwind and second order explicit schemes, respectively. SIMPLE-S (Semi-Implicit Method for Pressure Linked Equations–Simerics) algorithm is used to solve the pressure-velocity coupling equation [16, 17].

2.2 Translation dynamics model

A rigid body motion without considering the fluid-structure interaction is implemented in Simerics-MP+. This kind of dynamics needs conservation of linear momentum equation to be solved for translation rigid body motion.

The governing equation based on the conservation of linear momentum is given as

$$m\frac{d^2s}{dt^2} = F_{hydrodynamic} - F_{damping} - F_{spring} - F_{friction} + F_{additional} \tag{9}$$

In Simerics-MP+, the governing equation is solved for the displacement of the moving body along with the flow and cavitation governing equations.

Where, m is the mass of the moving body, s is the displacement of the moving body under the influence of the net force, $F_{hydrodynamic}$ is the fluid force due to pressure and shear forces, $F_{damping}$ is a damping force that can be due to damping action of a spring (if any) or due to any other external component, F_{spring} is a spring force, which is usually an opposing force, $F_{friction}$, is an opposing force due to frictional contact between the moving and the stationary bodies, $F_{additional}$ is any other external force acting on the moving body.

The displacement of the rigid body can also be prescribed as a constant value or a function of time. In this case, the linear momentum conservation equation is not solved.

2.3 Cavitation damage prediction model

Cavitation erosion, a phenomenon where high-energy release from imploding vapor bubbles can erode solid material, occurs under specific conditions. Bubbles form in zones where the pressure dips below the operating fluid's vapor pressure, only to collapse when they move to areas where the pressure exceeds this vapor pressure. This process of formation and implosion of bubbles in different pressure zones leads to cavitation erosion. In the solver, on a boundary of interest, the rate of change of cavitation bubble volume and bubble damage power are calculated. These two variables provide an indication of cavitation damage.

The rate of change of cavitation bubble volume is calculated as a total derivative with respect to time, which considers both the temporal and spatial variation of the bubble volume.

$$Bubble\ volume\ change\ rate = \frac{DV}{Dt} \tag{10}$$

Where, V is the volume of the bubble. The cavitation bubble damage power is calculated as

$$Cavitation\ bubble\ damage\ power = \frac{D(pV)}{Dt} \tag{11}$$

Where, p is the local pressure.

3 Mesh details

The fluid volumes are imported into Simerics-MP+ in stereolithography (STL) format. Fluid volume STLs are separated into stationary, moving (rotating or sliding), and deforming (valve ends) volumes. Fluid volumes are meshed using body-fitted binary tree mesh, which has several advantages [18] ranging from cubic cells offering orthogonality to an optimal transition between different length scales and resolutions. The Mismatched Grid Interface (MGI) feature in Simerics-MP+ is used to connect moving or stationary

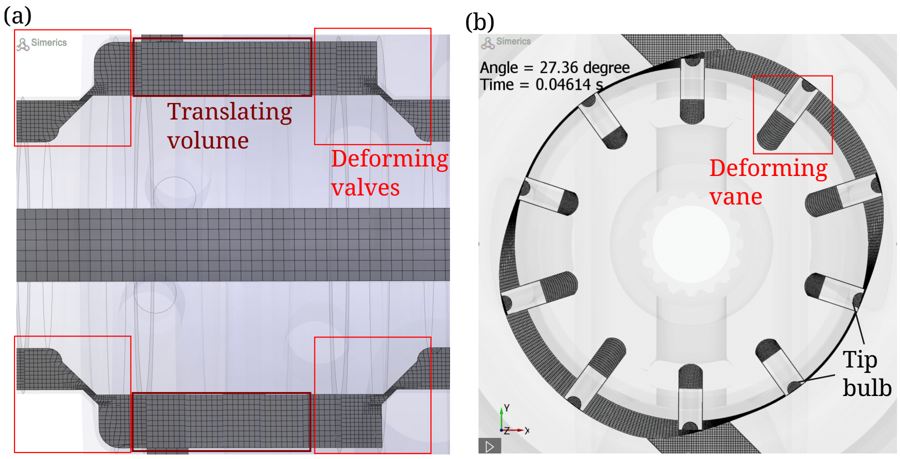

Figure 5 Cross section of (a) valve mesh showing translating and deforming meshes, and (b) vane mesh showing stationary, rotating and deforming meshes

neighbor mesh volumes. The deforming and moving meshes are changed internally every timestep by mapping the coordinates to a new coordinates based on the application by volume remeshing feature of Simerics MP+. For example, valves require expansion and contraction of the mesh coordinates, whereas pumps require rotation of the coordinates, which are handled internally by Simerics MP+ using volume remeshing feature.

Solenoid valves have valve bodies that translate in a single direction back and forth to seal the ports. In figure. 5 a, we point out the fluid volumes that are translating and deforming. The force interaction between the valve bodies and fluid is handled using the translation dynamic module. The translation module provides two methods for moving the valve bodies by remeshing: 1. Force balance mode that uses eqn. (9) where the valve moves on the basis of forces such as those of the spring and fluid acting on the valve bodies, and 2. prescribed motion mode that manually moves the valve body using valve displacement as a function of time.

A cross section of the vane pump mesh is shown in figure. 5 b. The vane pump model is setup using the “Vane” template of Simerics-MP+. The template enables the movement and deformation of the mesh in the vane volume as the vanes move with the rotor. In addition to remeshing volumes, it applies the appropriate boundary conditions, i.e. the rotation boundary condition, to the rotor surfaces. The template can also handle axial asymmetry in the rotor profiles with great ease. As the rotor rotates, the vane volume mesh compresses and expands depending on the distance between the cam, vane tip and rotor. The template can handle fixed-, variable-displacement, and balanced-vane configurations. In this study, we limit our scope to a balanced vane pump. The tip bulb dynamics is also simulated in this study using the "Radial Piston" template of Simerics-MP+. The Radial Piston template governs the mesh compression and expansion between the vane tip and the cam as the rotor rotates. The effect of spring loading on the vane motion and its effect of mesh compression and expansion between vane tip/cam as well as vane/rotor are also taken into account using the 1D translation dynamics module, similar to the valve mesh.

4 Results and discussion

In this section, we show the CFD simulation results of a few designs of a Parker Hannifin's valve and pump, used during the rigorous design process. Before the analysis, a grid independence study is performed to select the appropriate mesh for all the cases discussed. The appropriate mesh involves adequately resolving the annular, leakage, and side gaps in both the equipment. All the results presented have an error bar less than 5%, although they are not explicitly presented. All simulations are converged to 10^{-2} residual drop.

4.1 Solenoid Valve

4.1.1 Cavitation damage

In a solenoid valve, just when the valve body opens or closes the passages to allow or restrict flow, the flow velocity in the narrow passage is very high. Large velocities cause a massive pressure drop, and, when the pressure drops below the vapor pressure, cavitation bubbles form. This occurs predominantly in water-based equipment, such as this valve. The regions where such cavitation occurs is the narrow passage between the poppet seats and the cylinder surface as shown in the figure. 3, where the velocities are usually high. These cavitation bubbles often collapse when they enter the region of higher pressure. If cavitation bubbles collapse on the valve surfaces, they can damage the valve surfaces. When bubble collapses occur on poppet seats, sealing surfaces can be damaged, resulting in inadequate sealing. After repeated use of one of our prototype valves, we have observed cavitation damage marks on the sealing poppet surface, as shown in the figure. 6 a.

(a) (b)

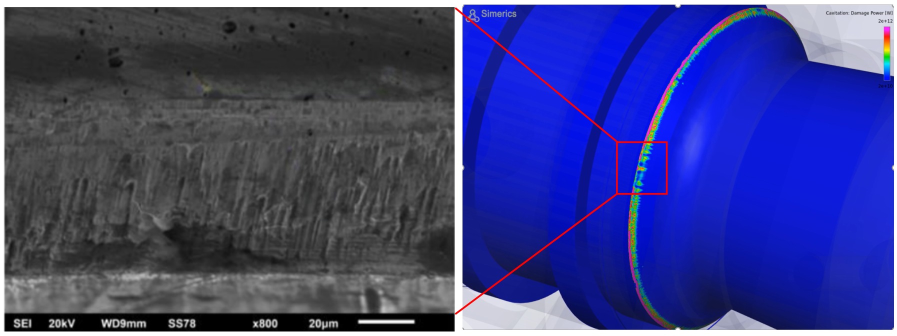

Figure 6 (a) Picture of pitting due to cavitation damage on the poppet surface removed from a valve after lab testing. (b) Cavitation damage power predicted by Simerics-MP+ on the poppet surface

Given that cavitation can shorten a valve's lifespan through metal surface erosion and induce high system vibration, it is crucial to engineer a valve design that minimally succumbs to cavitation. By leveraging 3D CFD, cavitation can be studied effectively using a variety of models coupled with the Navier-Stokes equation. We set out to use CFD to test the prototype that has shown cavitation damage in our experiments. The inlet boundary condition is kept at high pressure of 22.6 MPa, whereas the intermediate and outlet ports are at atmospheric pressure of 101 kPa. We use a constant gas cavitation model to account for cavitation and the translation dynamics model to move the valve bodies using prescribed motion. In this case, the valve body moves from right to left with reference to the figure 3.

We present the figure. 6 b that shows the damage power calculated by Simerics MP+ as a result of bubble collapse on the poppet, when the valve is just opening. The simulation clearly points out that the cavitation damage would occur on the poppet seat, which is in agreement with the pictures shown previously in the figure. 6 a. Since CFD can be a reliable tool for studying cavitation, it can be used to test various designs to find designs that show minimal cavitation damage. In addition to identifying potential cavitation damage areas, cavitation models contribute key physics to a CFD model that can improve overall accuracy of global parameters such as outlet pressures and volumetric flow rates.

4.1.2 Valve body forces

The forces that act on the valve bodies at any given time are the spring and fluid forces. Fluid forces can be categorized into shear forces and pressure forces. When the valve moves, the pressure forces dominate the shear forces due to the immense pressure range (22.6 MPa to 101 kPa) at which these valves operate. These pressure forces, in addition to the spring forces that act on the valve bodies, dictate whether a given valve would operate as expected. In other words, during the movement of the valve body, fluid pressure forces and spring forces can either support or oppose the valve motion. Hooke's law typically provides a straightforward calculation for the spring forces, leaving the fluid pressure forces as the only forces to be determined in order to predict the motion of the valve.

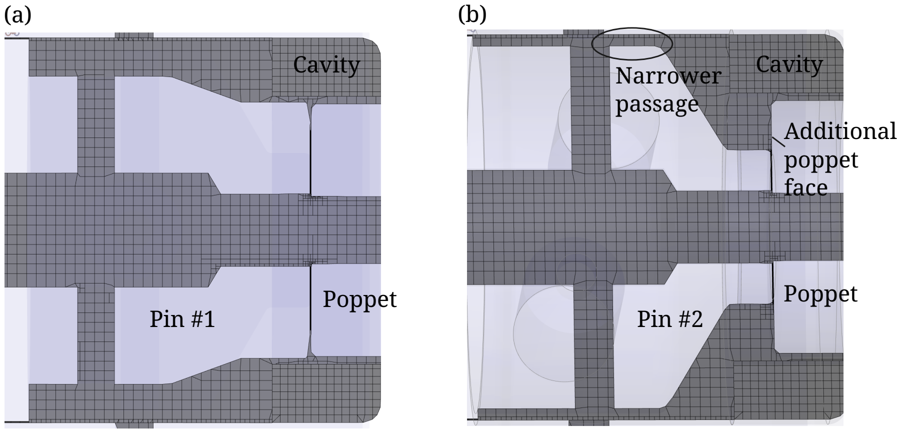

Figure 7 Mesh zone between pin and poppet of (a) #1 pin design, and (b) #2 pin design.

To highlight the importance of studying fluid pressure forces, we present two design concepts of the pin that have been used in Parker Hannifin's meticulous design process in figure. 7 a and b. The second design has two key differences: 1. an additional surface on the poppet body in the cavity where pin and poppet touch each other, and 2. the passage connecting the valve chamber and the intermediate ports is narrower. During laboratory tests, we have observed that when the solenoid is actuated, both designs work as expected, i.e. the valve bodies move from the right valve seat to the left with reference to the figure. 3. However, when the solenoid is turned off, the first design sometimes has difficulty moving the valve body from left to right due to valve instability and hence the inlet and the intermediate ports stay connected. This is not observed in the second design. Since the spring forces are the same between the two designs, the fluid pressure force is the only difference between the two designs and needs to be investigated.

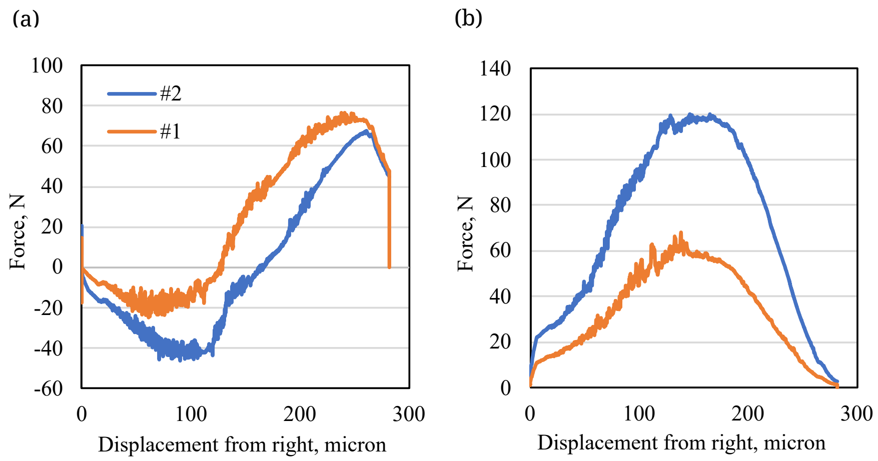

Figure 8 Forces on (a) the poppet and (b) the pin, for two pin designs when valve moves from right to left. Positive force promotes the valve motion in the desired direction

We have performed CFD simulations to predict fluid pressure forces on the valve bodies. To simplify the simulations, we assume that the three valve bodies move together, although it is possible for the valve bodies to separate and combine when traveling. Since we know the valve movement time from the tests, we have used prescribed motion to move the valve manually over $0.5s$, without considering any spring forces. For the intermediate, inlet and outlet port pressure boundary conditions, we use the test data measured by the pressure transducers. We use the same numerical models we used in the cavitation study shown in the previous section. To find the pressure forces on the valve body, we compute the integral of the pressure over the valve body area. We present forces with sign convention such that the positive force helps move the valve in the desired direction, whereas the negative force hinders the valve from moving in the desired direction.

In figure. 8a and b, we present the pressure force on poppet and pin bodies respectively as a function of valve displacement, when the solenoid is actuated i.e. when the valve bodies move from right valve seat to left valve seat. In both designs, fluid forces mostly encourage the solenoid to move the valve bodies in the desired direction. The forces on the poppet and the pin are different in magnitude but have the same direction meaning, there is a possibility of valve bodies splitting but still moving in the desired direction. Note that the highest hindering force occurs in the poppet when the displacement is around 100 microns. We hypothesize that the hindering force can be overcome by the poppet's spring force of 40 N since they are of the same order. It is also important to note that during force-balanced valve body motion, the inertial forces of valve bodies can also work with spring force to overcome undesirable fluid forces. These reasons could potentially explain why both designs have performed well when the solenoid is actuated during lab tests.

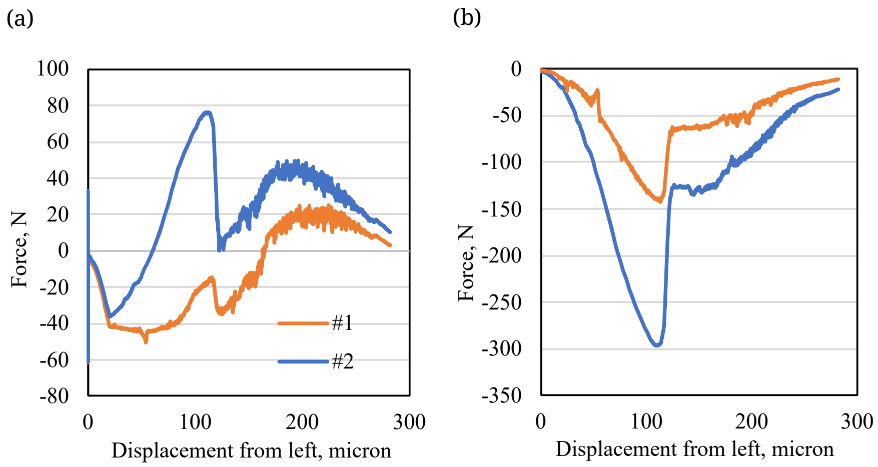

Figure 9 Forces on (a) the poppet and (b) the pin for two pin designs when valve moves from left to right. Positive force promotes the valve motion in the desired direction.

When the solenoid is switched off, there is no more solenoid force to keep the valve bodies on the left valve seat. The spring forces on the valve bodies will tend to push the valve back to the right. Figure 9 a shows the fluid forces on the poppet, for both designs. The poppet on the first design experiences a force that opposes the movement of the valve body. Unlike previously where the poppet's spring force has helped the poppet overcome fluid resistance, here the poppet's spring force is $-40N$, which does not help the poppet move in the desired direction. However, for the second design, the fluid forces mostly encourage the movement of the poppet. This could explain why the second design performed better than the first in the tests. In figure 9 b that shows the forces on the pin of two designs, we point out that the pin forces are acting in the undesired direction. The pin is pushed towards the left, while the poppet is moving towards the right, as we observe in Figure

9 a. These opposing forces can cause the poppet and pin to split and move in opposite directions. However, this will not affect the function of the valve because the poppet that does the actual sealing tends to move in the desired direction.

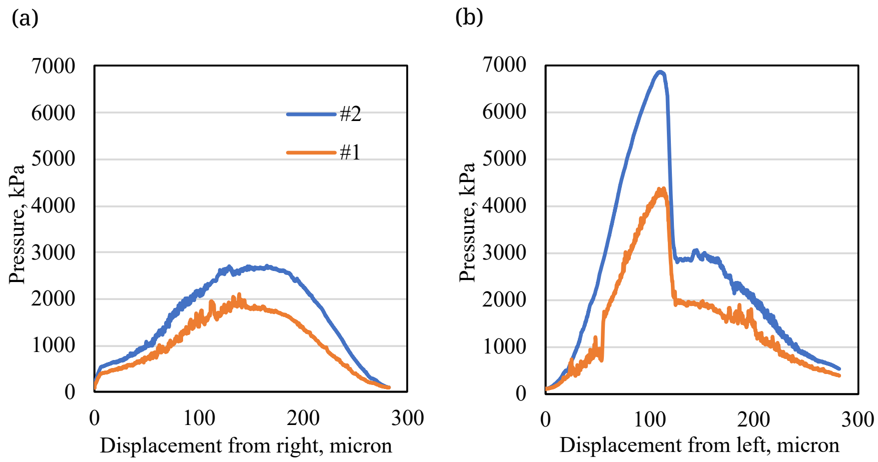

Figure 10 Cavity pressure as a function of displacement for two poppet designs when the solenoid is (a) on and (b) off

To explain the differences in forces between the pin and the poppet, we now examine the cavity between the poppet and the pin. In fact, the pressure built up in this cavity can influence the forces of the valve bodies, and therefore the splitting of the valve bodies. The figure. 10 a shows the cavity pressure of two designs when the valve body moves from right to left. Both designs show similar trends, and the second design has higher cavity pressures. We observe the same phenomenon in the figure. 10 b when the valve body moves from left to right. This can be explained by the narrow passage in the second design. The narrow passage of the second design can throttle the flow, resulting in pressures higher than those of the first design. Also, the higher cavity pressures in the second design is a plausible explanation for why we observe larger forces overall for the second design in the figures. 8 and 9. To visualize the high and low cavity pressures in the first and the second designs, respectively, we present the figure. 11 a and b when the valve bodies move from left to right at displacement of 100 microns from the left valve seat.

In both designs, when the valve bodies are moving towards the left, we hypothesize that the cavity pressure imparts forces on the valve bodies and hence is responsible for splitting the valves. However, these cavity pressures are not high enough to impose opposing forces on the pin and the poppet to move them in the oppposite direction. When the valve bodies move towards the right, the cavity pressure reaches as high as 6894 kPa for the second design as shown in figures 10 b and 11 b. The second design also has an additional surface on the poppet side of the cavity as a design feature as seen in figure. 7 b. We hypothesize that high cavity pressures impart massive forces on the poppet's additional surface and the pin, as seen in figure 9 a and b. This could result in splitting of the pin and poppet, moving them in opposite directions, specifically pushing the poppet in the desired direction. Massive cavity pressure and an additional poppet surface are absent in the first design, as seen in the figures. 10 b, 11 b, and 7 c. Hence, the first design did not have adequate desirable force to move the poppet in the desired direction, when the solenoid is turned off.

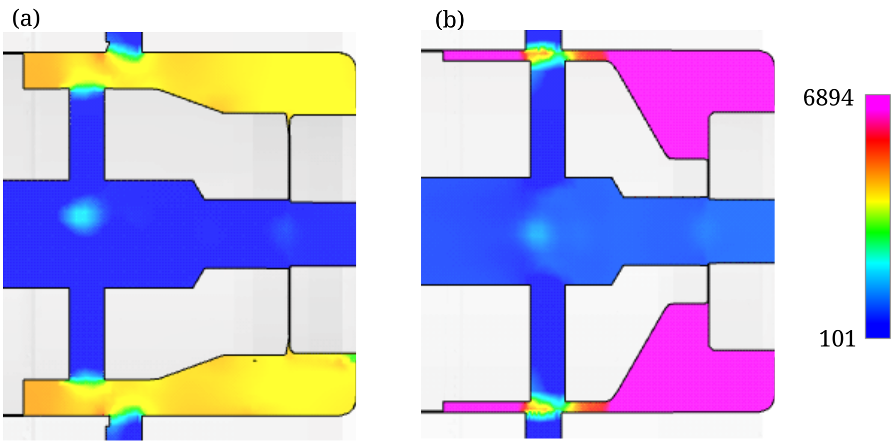

Figure 11 Comparison of cross sections of cavity pressure between designs (a) #1 and (b) #2 when displacement is 100 micron from the left. The unit for pressure used is kPa.

4.1.3 Valve separation

Since we have hypothesized that valve bodies can split based on cavity pressure in the previous section, it could be worthwhile to simulate valve separation and see what influence valve separation can have on flow dynamics. To demonstrate valve body separation, we have performed a transient dynamic simulation of a solenoid valve with the second poppet design shown in Figure 7 b, where the poppet and pin can split and combine depending on the fluid forces. To do this, we alter the model to employ a translation dynamics model that incorporates force balance, as opposed to the previously used method of prescribed motion. The model now takes into account the forces of the spring and solenoid. The valve bodies now move solely as a result of spring, solenoid, and fluid forces. The starting position is the right, i.e. the solenoid is being actuated to move the valve bodies to the left with reference to figure. 3.

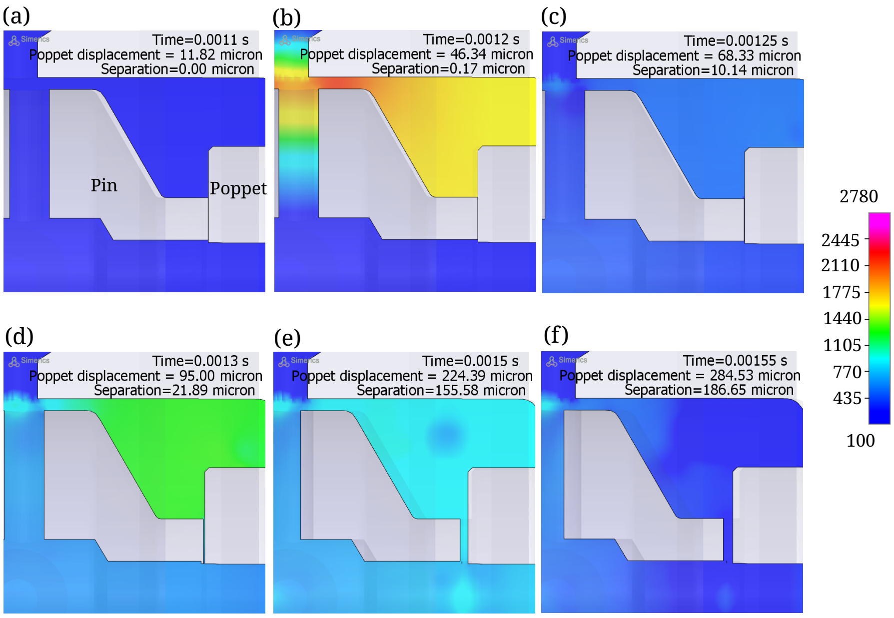

Figure 12 Cross sections showing cavity pressure and valve body splitting: (a) Cavity inadequately pressurized by inlet pressure due to small poppet displacement of 11.82 μm. (b, c, d, e) Cylclic increase and decrease in cavity pressure as the pin and poppet start separating. Cavity is adequately pressurized by inlet as the poppet is still traveling to the left, leaving cavity and inlet port connected. (f) Pressure is fully relieved as the high pressure source is disconnected by the poppet. The poppet has reached its final destination and the its displacement is 284.53 μm. Unit for pressure is kPa.

Figure. 12 a shows the pressure contour just when the poppet starts moving. At this point the cavity pressure is inadequate to cause valve splitting but that would change as the poppet moves. As time goes on and the poppet moves, the cavity pressure builds because the cavity is now connected to the high pressure inlet. This increase in cavity pressure leads to valve splitting and the pin moves further away as shown in figure 12 b. This valve body separation is due to the balance of force between spring, solenoid, and fluid forces. As the valve splits, the cavity pressure starts to relieve itself through the central line. So, we notice a lower pressure in figure 12 c. Then the cavity is pressurized further by the inlet, and the pressure increases as we see in figure. 12 d which further causes more splitting. But this time, the leakage between the cavity and the central line is preventing the pressure from rising to larger pressures we observe in the figure. 12 b. This process of increasing pressure and moving the pin body only to relieve it happens again and again as shown in the figure. 12 b to e until the poppet finally reaches the other side and the pressure is completely relieved in the end.

It is important to note that, despite separation, both the poppet and pin move in the desired direction as evident in the figure. 12. This mirrors our earlier hypothesis from the previous section, where we calculated the forces exerted on the valve bodies as it moved from right to left in a prescirbed motion, without undergoing any separation. Although modeling valve body separation has not changed the earlier hypothesis, it could be a valuable modeling methodology to accurately predict valve body forces, since fluctuating cavity pressure seen in the figure. 12 could cause fluctuating valve body forces.

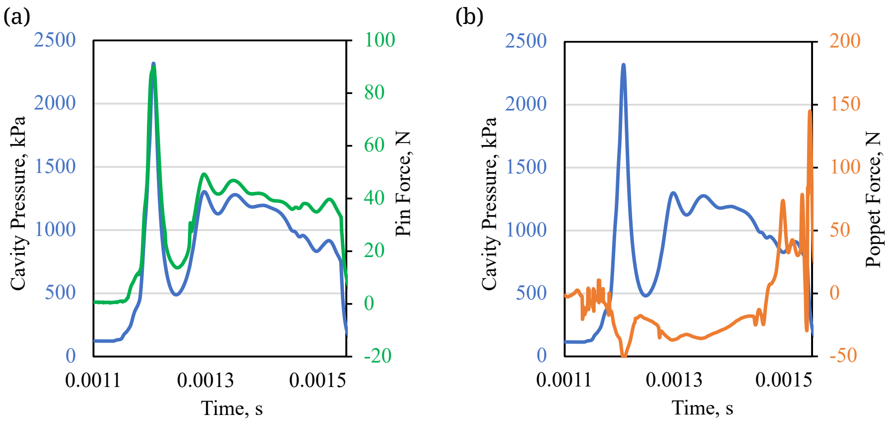

Figure 13 Cavity pressure during valve splitting period plotted against (a) the force on the pin and (b) the force on the poppet. Positive force promotes the valve body motion in the desired direction.

To show the fluctuating forces on the valve bodies: the pin and the poppet, due to fluctuations in the cavity pressure, we present the figure. 13. The cavity pressures and forces of the valve bodies are plotted for the duration when valve separation occurs. Like mentioned previously, the positive force helps move the valve body in the desired direction. In figure. 13a, we have quantified the pressure fluctuation visualized in the figure. 12. In addition, the forces on the pin fluctuate in a similar fashion to the cavity pressure. The cavity pressure has a strong positive correlation with the forces on the pin. Similarly, the forces on the poppet fluctuate with cavity pressure as seen in the figure. 13b. However, the cavity pressure has a negative correlation with the forces on the poppet. This is understandable because the cavity pressure tends to push the valve bodies away from each other in opposite directions because of its location as seen in the figure. 12a. In other words, high cavity pressures push the pin towards the desired direction, whereas the poppet in the undesired direction. This becomes evident when the figures. 13a and b are compared.

4.2 Vane pump

In this section, we discuss the design improvement made by Parker Hannifin on one of the vane pumps after several CFD studies conducted in Simerics MP+. During the design process, we identify critical flow characteristics that need to be optimized and do several iterations of design change to arrive at a design that has improved performance.

4.2.1 Critical flow characteristics

To identify critical flow characteristics, we set out to perform a CFD simulation of the base design of a vane pump using the equilibrium dissolved gas cavitation and turbulence models for the flow; the translation model is used for the movement of the vane inside the slots.

Suction regions often experience pressures lower than the vapor pressure, resulting in cavitation. Figure 14 a shows this clearly in the suction region as large vapor volume fraction computed by CFD. In addition to typical cavitation in the suction region, the vane pump has an additional region where cavitation occurs. As the rotors rotate, the vanes can move radially due to the centrifugal, hydraulic pressure and spring forces. Using the dynamics model of Simerics MP+, we are able to appropriately model the vane motion as a result of force balance. During the motion of vanes, the pockets enclosed by the vane and rotor in the suction regions expand. Figure. 14 a and b show the expansion of a pocket based on rotation. In this zone, pressures can go below vapor pressure, and hence cavitation bubbles can form. The cavitation that occurs as a result of the expansion of the vane cavity can be realized when

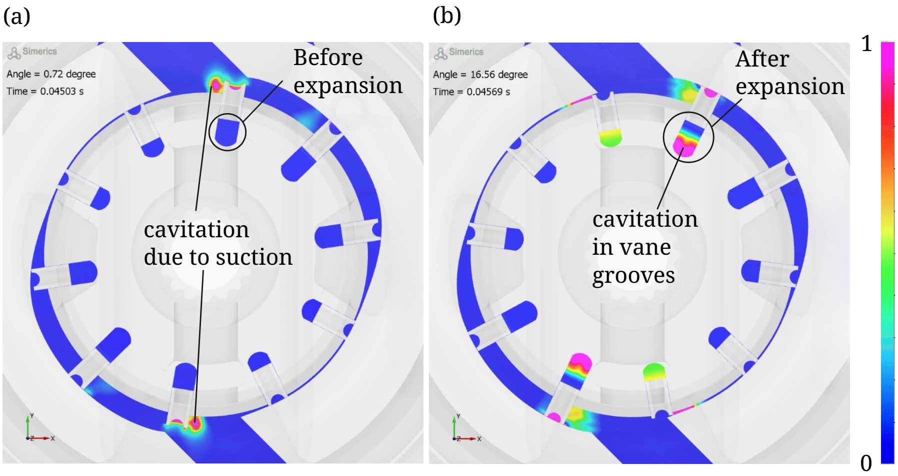

Figure 14 Cross section of vapor volume fraction of the base design of a vane pump. (a) Cavitation near suction port. (b) Cavitation in the vane slot as the vanes in suction region move outwards causing pressure drop.

the vapor volume fractions of the vane cavity before (figure. 14 a) and after expansion (figure. 14 b) are compared.

Another critical flow characteristic is the velocity profile at the inlet and outlet ports. Figure. 15 a shows the instantaneous velocity profiles for inlet and outlet ports. Although the inlet velocity profiles are smooth, the outlet velocity profiles are turbulent, and the local velocities are higher in certain regions. Turbulent vortices in the outlet can cause energy dissipation and therefore reduce the efficiency of the vane pump. The reasons for turbulent vortices and large local velocities are steps and narrow passages, respectively, as highlighted in the figure 15 a.

Lastly, leakage gaps also play a role in reducing efficiency. At higher speeds and pressure, leakages between the inlet and outlet ports become predominant and could largely reduce the volumetric flow rate of a pump. Leakages between the rotor and the housing and the vanes and the slots are shown in the figure. 15b.

By modifying the suction, discharge, and leakages appropriately in the base design, one can reduce cavitation, turbulent vortices, and high local velocities, and thereby improve the performance of the vane pump. After a rigorous parametric study on dimensions of vane grooves, inlet and outlet ports using CFD, we have arrived at an optimized design with higher efficiencies and discharge pressures. Using the base and optimized design,

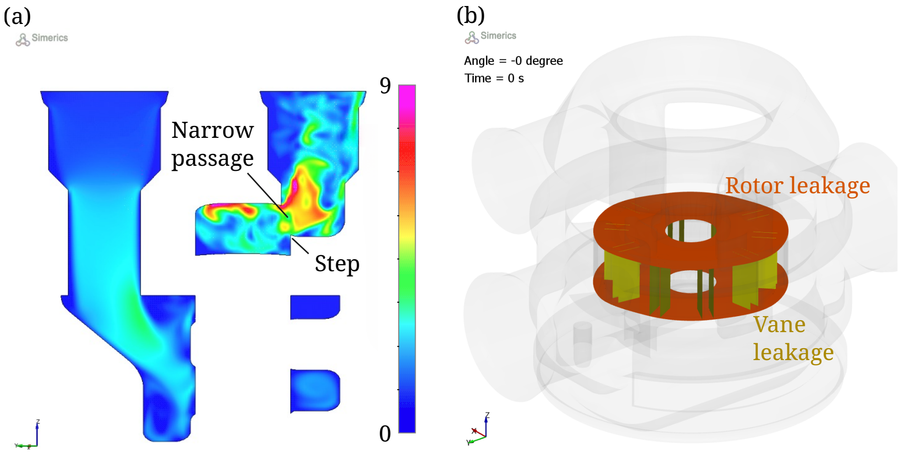

Figure 15 (a) Velocity patterns in inflow and outlflow. Unit of velocity is ms^{-1} (b) Rotor and vane leakage gaps.

prototypes have been built, and experiments have been conducted to verify the improvement in performance.

4.2.2 Comparison of base and optimized designs using experiments

In the experiments, we start by testing the dependence of discharge flow rates on rotation speeds at an suction pressure of 80 kPa. We anticipate the output flow to increase linearly with speed until a certain speed is reached, after which cavitation or leakages become predominant and the flow rate does not increase linearly anymore. We call that speed the maximum running speed of the base design and use it to non-dimensionalize the speed of both base and the improved design. We also call the flow rate that corresponds to this maximum speed the maximum flow rate since this is the highest flow rate one can expect from the base design before cavitation or leakages becomes predominant. We use this flow rate to non-dimensionalize the flow rate measured in both the base and the improved designs. We also non-dimensionalize discharge pressure by maximum operating discharge pressure of the base design. By non-dimensionalizing parameters based on the base design's maximum operating condition, we make it easier to visualize the improvements from the base design.

Figure. 16 a shows the non-dimensional flow rate (V') as a function of the non-dimenstional speed (ω') of the base (red) and optimized design (blue) at an intake pressure of 80 kPa and discharge pressure of 1500 kPa. We notice in

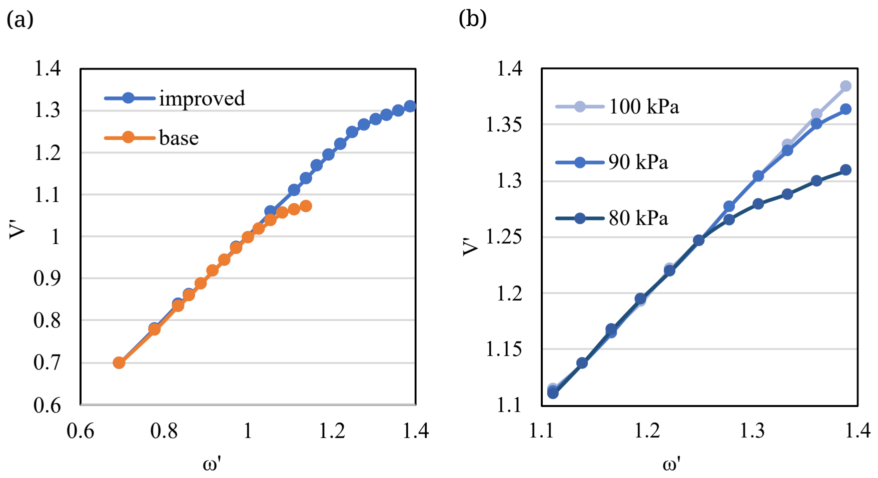

Figure 16 (a) Non-dimensional flow rate as a function of non-dimensional speed for base and improved design for suction pressure of 80 kPa. (b) Non-dimensional flow rate as a function of non-dimensional speed for various suction pressure in the extended working range.

the base design that the flow rate varies linearly with speed as intended until $(1, 1)$. Data corresponding to $(1, 1)$ of the base design belong to the maximum operating conditions above which cavitation and leakages becomes predominant. The data point in the improved design that is equivalent to $(1, 1)$ of the base design is $(1.138, 1.15)$. This signifies that the operating speed of the optimized design has increased by 13.8% and the highest volumetric flow rate by 15%, compared to the base design. To show the flow rate dependence on suction pressure in the extended operating range of the improved design, we present figure. 16 b. As expected, for higher inlet pressures, the performance drop does not occur until much later speeds, as larger suction pressures inhibit cavitation bubble formation and also cause smaller leakages.

To compare the effect of discharge pressures on efficiency, we have performed a different set of tests in which we vary the speed and discharge pressures to measure the volumetric flow rate in the outlet. We set the suction pressure at 100 kPa. Using the theoretical and measured volumetric flow rate, the volumetric efficiency is calculated and presented as a color contour for various non-dimensional speed (ω') and non-dimensional discharge pressures (P'_{out}) in the figure. 17. First, we point out that the improved design has an overall higher efficiency than the base design. Second, the operating speed and discharge pressure ranges have increased by 39% and 6% respectively, in the improved design, as seen in the figure 16 a. Finally, we see remark-

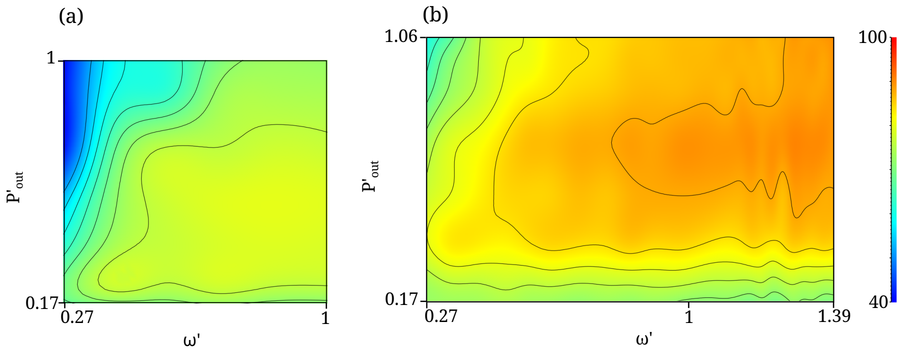

Figure 17 Contours showing efficiency for various discharge pressure and vane speed for (a) base design and (b) improved design. Improved design shows extended discharge pressure and working speed ranges.

ably higher efficiencies even at high discharge pressures and extended speed ranges.

To compare the simulation results with experimental data, we present non-dimensionalized volumetric flow rates of the improved design at different non-dimensionalized discharge pressures for experiments and simulations in the figure. 18a. The inlet is maintained at 101 kPa. At lower discharge pressures, the simulation results and the experimental results vary more than when the discharge pressures are higher. At low discharge pressure, the discharge velocities are usually large. The high discharge velocities cause swirling flows, which are often difficult to simulate. Nevertheless, the margin of error is very low, as shown in the figure. 18b. The highest percentage error observed between the simulations and the experiments is 2.50%, which is well within the acceptable range for engineering applications.

5 Conclusion

In this paper, we have discussed two hydraulic equipment: a solenoid valve and a vane pump that are being used in subsea and off-highway applications, respectively. All solenoid valve designs and vane pump designs used have been part of Parker Hannifin's rigorous design process.

In the solenoid valve section, we have shown how CFD can be used to predict cavitation damage in critical areas of the valve. It has also been shown that CFD serves as an instrument to elucidate the phenomena noted in the experimental studies of two valve designs. Simulations involving complex

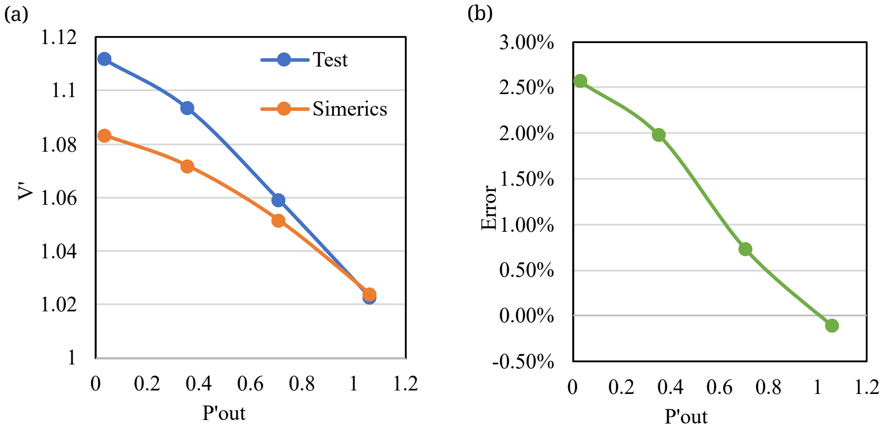

Figure 18 (a) Non-dimensionalized volumetric flow rate at different non-dimensionalized discharge pressures of the improved pump. (b) Difference between test and simulation results quantified as percentage change for various discharge pressures.

transient dynamics, such as valve separation, have been performed using the comprehensive rigid body dynamics offered by Simerics MP+. This only shows how advanced CFD along with transient dynamics and data analytics can be used to simulate phenomena that are nearly impossible to study in experiments. These studies have allowed Parker Hannifin to perform targeted optimizations, mitigating cavitation risks, a common issue in subsea applications that can lead to reduced efficiency and potential damage over time, and improving valve stability.

In the next section, we have modeled a vane pump and the transient dynamics of vane motion inside the slot, using pre-coded templates in Simerics MP+. This has helped identify flow attributes, notably cavitation within vane slots. By altering the geometries and utilizing CFD to choose a superior design, we have managed to enhance the total performance of a pump by boosting both the operational range and efficiency. This advancement propels us closer to realizing a cost-efficient off-road electric-hydraulic mobile system, marking a significant stride in Parker Hannifin's path towards electrification.

This paper has demonstrated the transformative impact of integrating advanced CFD simulation tools such as Simerics MP+ into the hydraulic fluid power engineering design process. Through meticulous validation and verification, upfront modeling of complex transient dynamics, and strategic optimization of key components, we have demonstrated the potential of simulation-driven engineering to address and solve some of the most challenging problems in the field. Our successful application of these advanced techniques in comprehending the complex transient dynamic behavior in a subsea solenoid valve and a vane pump sets new benchmarks in product design and development of subsea and off-highway equipment.

References

[1] K. Sotoodeh, "A review on subsea process and valve technology," in *Marine Systems & Ocean Technology*, vol. 14, pp. 210–219, 2019.

[2] AMPP, "Nace standards resource," 2024. `https://www.ampp.org/standards/ampp-standards/standards-resources` [Accessed: April 8th 2024].

[3] API, "Api standard - 17f," 2024. `https://www.api.org/~/media/files/publications/whats%20new/17f%20e3%20pa.pdf` [Accessed: April 8th 2024].

[4] M. Solnørdal, "Hydrogen induced stress cracking (hisc) and dnv-rp-f112," in *Measurement and Control*, vol. 42, pp. 145–148, 2009.

[5] H. Zhang and R. Nagel, "Electrification challenges and solutions in mobile system design," 2023.

[6] F. Nishanth, G. Bohach, J. Van de Ven, and E. L. Severson, "Design of a highly integrated electric-hydraulic machine for electrifying off-highway vehicles," in *2019 IEEE Energy Conversion Congress and Exposition (ECCE)*, pp. 3983–3990, IEEE, 2019.

[7] F. Un-Noor, G. Wu, H. Perugu, S. Collier, S. Yoon, M. Barth, and K. Boriboonsomsin, "Off-road construction and agricultural equipment electrification: Review, challenges, and opportunities," *Vehicles*, vol. 4, no. 3, pp. 780–807, 2022.

[8] J. R. Valdes, J. M. Rodríguez, R. Monge, J. C. Peña, and T. Pütz, "Numerical simulation and experimental validation of the cavitating flow through a ball check valve," *Energy Conversion and Management*, vol. 78, pp. 776–786, 2014.

[9] L. Li, H. Zhang, G. Davis, F. Kalb, and S. Hamid, "Improving the closing characteristics of subsurface safety valve with combined fea and cfd modeling/numerical analysis," in *SPE western regional meeting*, pp. SPE–93941, SPE, 2005.

[10] E. Frosina, A. Senatore, D. Buono, M. Pavanetto, M. Olivetti, and I. Costin, "Improving the performance of a two way flow control valve, using a 3d cfd modeling," in *ASME International Mechanical Engineering Congress and Exposition*, vol. 46545, p. V007T09A085, American Society of Mechanical Engineers, 2014.

[11] E. Frosina, A. Senatore, D. Buono, K. A. Stelson, F. Wang, and H. Gao, "A three-dimensional cfd methodology to study vane-ring and vane-under-vane interactions of a vane pump power split transmission," in *Fluid Power Systems Technology*, vol. 50473, p. V001T01A042, American Society of Mechanical Engineers, 2016.

[12] B. Kashid and M. Eichler, "Lies, damned lies, and simulation results: How to change the conversation and build a thriving simulation ecosystem," in *Offshore Technology Conference*, p. D012S059R003, OTC, 2021.

[13] J. Azar, "Oil and natural gas drilling," in *Encyclopedia of Energy* (C. J. Cleveland, ed.), pp. 521–534, New York: Elsevier, 2004.

[14] A. K. Singhal, M. M. Athavale, H. Li, and Y. Jiang, “Mathematical basis and validation of the full cavitation model,” *Journal of Fluids Engineering*, vol. 124, no. 3, pp. 617–624, 2002.
[15] Simerics Inc., “Simerics-MP+ user manual,” 2024.
[16] A. Pandey, J. Wang, D. Maiti, and Y. Jiang, “Performance and validation of a segregated pressure-based solver for computations of low and high-speed compressible flows,” in *AIAA SCITECH 2023 Forum*, p. 2274, 2023.
[17] S. Taghizadeh, K. C. Ng, J. Horen, and S. Dhar, “A 3d computational fluid dynamics and acoustics simulation approach for noise mitigation prediction in gerotor pumps,” tech. rep., SAE Technical Paper, 2024.
[18] H. Ding, F. Visser, Y. Jiang, and M. Furmanczyk, “Demonstration and validation of a 3d cfd simulation tool predicting pump performance and cavitation for industrial applications,” *Journal of Fluids Engineering*, 2011.